Wave Guiding Properties of Large Low-Conductivity Cylinders

Shota Ueda, Masahiro Hasegawa, Yoshihiro Baba¹⁰, Fellow, IEEE, and Vladimir A. Rakov¹⁰, Fellow, IEEE

Abstract—Using the FDTD method for solving Maxwell's equations, we have studied wave guiding properties of a large cylinder, having a radius of 100 m, $\varepsilon=\varepsilon_0$, and $\mu=\mu_0$, for four values of conductivity, $\sigma = \infty$, 10^{-3} S/m, 10^{-4} S/m, and 10^{-5} S/m. The cylinder was excited by a Gaussian voltage pulse whose half-peak width (HPW) was 1, 3 or 10 μ s. In all considered cases, traveling waves were observed and the longitudinal Poynting vector P_z on the cylinder surface was greater than (or comparable to for HPW = $1 \mu s$) the radial Poynting vector P_r . The wave propagation speeds were of the order of 10^8 m/s. Even for $\sigma = \infty$, traveling current waves exhibited attenuation, which was not much different for $\sigma =$ 10^{-3} S/m and was noticeably stronger for lower values of σ . After propagation over 400 m, the current peak was about 70% to 90% of its original value for $\sigma = \infty$, about 60% to 80% for $\sigma = 10^{-3}$ S/m, about 40% to 60% for $\sigma=10^{-4}$ S/m, and about 10% to 20% for $\sigma=10^{-5}$ S/m. The current attenuation distances, over which the amplitude decreases to 1/e (about 37%) of its original value, for $\sigma = 10^{-5}$ S/m were roughly 120, 170, and 220 m for HPW = 1, 3, and 10 μ s, respectively. The results imply that essentially cold and, hence, low-conductivity compact intracloud discharges (CIDs), whose lengths are usually a few hundreds of meters may involve traveling wave phenomena, such as reflections.

Index Terms—Attenuation distance, finite-difference time-domain (FDTD) method, low-conductivity cylinder, poynting vector, reflection, traveling wave, waveguide.

I. INTRODUCTION

B ABA and Rakov [1] examined the mechanism of attenuation of current wave as it propagates along a perfect conductor of nonzero thickness. They have found that the current attenuation is due to electric field scattering that occurs in order to satisfy the boundary condition on the tangential component of electric field on the conductor surface. They also approximated a vertical conductor above ground by a nonuniform transmission line (TL) whose characteristic impedance increases with increasing height and showed that it reasonably reproduces the current wave attenuation predicted by the scattering theory. In the TL approximation, the current attenuation with height can

Manuscript received 23 February 2024; revised 19 April 2024; accepted 21 May 2024. Date of publication 12 June 2024; date of current version 15 August 2024. This work was supported in part by U.S. National Science Foundation under Grant AGS-2055178 and Grant AGS-2426833. (*Corresponding author: Yoshihiro Baba.*)

Shota Ueda, Masahiro Hasegawa, and Yoshihiro Baba are with the Doshisha University, Kyoto 610-0394, Japan (e-mail: ctwk0351@mail4.doshisha.ac.jp; ctwh0309@mail4.doshisha.ac.jp; ybaba@mail.doshisha.ac.jp).

Vladimir A. Rakov is with the University of Florida, Gainesville, FL 32611-6130 USA (e-mail: rakov@ece.ufl.edu).

Color versions of one or more figures in this article are available at https://doi.org/10.1109/TEMC.2024.3408849.

Digital Object Identifier 10.1109/TEMC.2024.3408849

be attributed to the distributed impedance discontinuity causing distributed reflections back to the source.

TL approximation is often used in the modeling of traveling waves occurring in various lightning processes (e.g., Uman and McLain [2]; Gorin [3]; Rakov and Uman [4]; Nag and Rakov [5]; De Conti et al. [6]; and Tran and Rakov [7]). Some TL models are based on solving differential telegrapher's equations, which may include ohmic losses, nonuniformity, and nonlinearity, while others are of engineering type, in which the current traveling wave is specified directly. In most cases, a hot lightning channel with conductivity of the order of 10⁴ S/m is assumed or implied, although Rakov [8] additionally considered a pre-dart-leader channel with conductivity of 0.02 S/m.

Engineering models of traveling-wave type have been also applied (e.g., Nag and Rakov[5]; Rison et al.[9]; and Li et al.[10]) to the so-called compact intracloud discharges (CIDs), which are very different from the ordinary lightning discharges. Specifically, CIDs are expected to be essentially cold (< 1000 to 2000 K or so) streamer formations, so that their conductivity is orders of magnitude lower than that of hot (> 5000-6000 K or so) and even decayed (about 3000 K or so) channels traversed by ordinary-lightning processes. Further, the transverse dimensions of CIDs are expected to be of the order of tens to hundreds of meters, much larger than for ordinary lightning, while their longitudinal dimensions are some hundreds of meters. The estimates of conductivity of various streamer formations, composed of numerous streamers at different stages of development, reported by Maslowski and Rakov [11], Rakov and Tran [12], and Bogatov et al. [13] (further discussed in Section IV) suggest that the conductivity of CIDs is of the order of 10^{-5} S/m. Nag and Rakov[14] estimated the range of CID current zero-to-peak risetimes to be from about 2 to 10 μ s with an average of 5 μ s. The corresponding 10%–90% risetimes ranged from about 1 to 6 μ s with an average of about 3 μ s. It is presently not clear if a cylinder of, say, 100-m radius and conductivity of 10^{-5} S/m could act as a guiding structure for traveling current waves associated with CIDs.

In this article, using the finite-difference time-domain (FDTD) method [15], we study wave guiding properties (propagation speed, attenuation distance, etc.) of large low-conductivity cylinders, in order to check if such cylinders, roughly representing essentially cold CIDs, could support traveling waves. Other aspects of CIDs, including possible nonuniformities and nonlinearities, are outside the scope of this article. An overview of the current knowledge on CIDs can be found in Rakov et al. [16] and in references therein.

0018-9375 © 2024 IEEE. Personal use is permitted, but republication/redistribution requires IEEE permission. See https://www.ieee.org/publications/rights/index.html for more information.

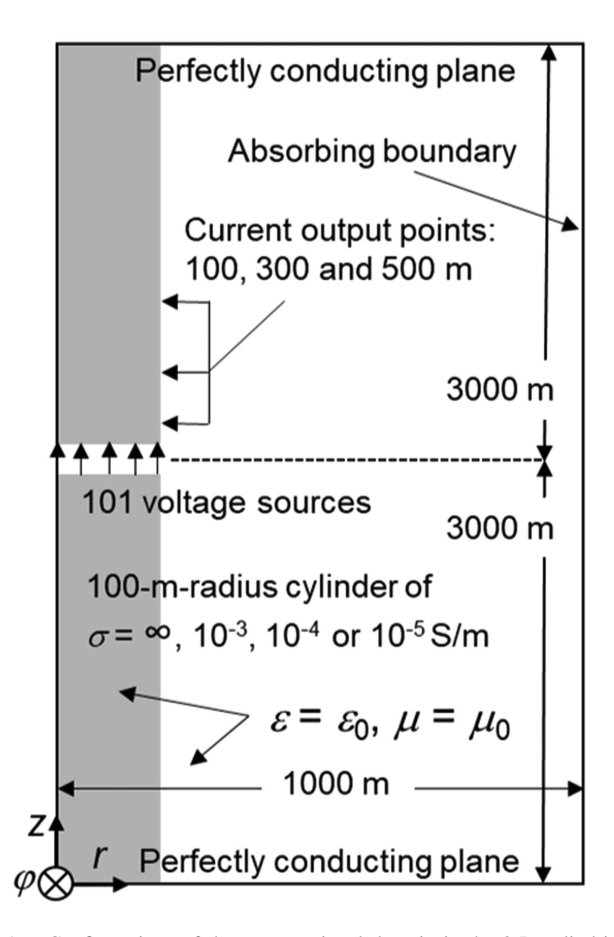


Fig. 1. Configurations of the computational domain in the 2-D cylindrical coordinate system.

II. MODEL DESCRIPTION

Fig. 1 shows the configuration used in the FDTD simulations in the two-dimensional (2-D) cylindrical coordinate system. The 2-D computational domain, whose radial dimension is 1 km and vertical dimension is 6 km, is divided into square cells of $\Delta r =$ $\Delta z = 1$ m. The time increment is set to 1 ns. Liao's second-order absorbing boundary condition [17] is applied to the right-side boundary to minimize unwanted reflections there. The upper and lower boundaries are set to be perfectly conducting planes. The left-side boundary (z-axis) coincides with the axis of the cylinder, whose radius and length are 100 m and 6 km, respectively. The reason for using such a long cylinder is to avoid/reduce the influence of reflections from the ends of the cylinder. Four constant values of conductivity, $\sigma = \infty$, 10^{-3} S/m, 10^{-4} S/m, and 10^{-5} S/m were used. The latter value is the best available estimate for streamer formations near ground level [11], [12], [13], and the other three values are included just for comparison. It is possible that the conductivity of streamer formations inside the cloud can be somewhat lower because of lower air density, but this is unlikely to alter our main conclusions. Both the relative permittivity and relative permeability were set to unity for the entire computational domain.

The vertical cylinder is excited by 101 voltage sources placed in a 1-m gap equidistant from its ends and uniformly distributed (1 m apart in the radial direction) over the cross-section of the

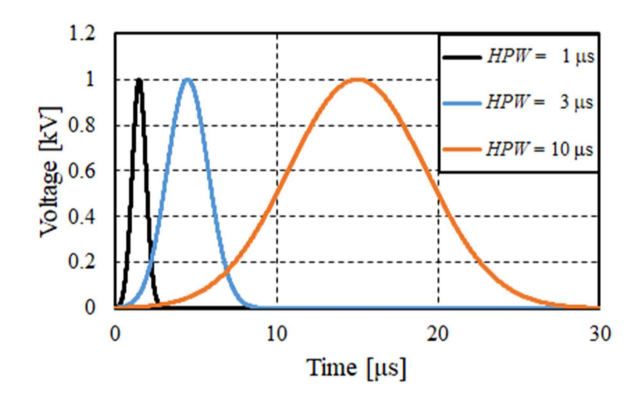


Fig. 2. Three excitation voltage waveforms with HPWs of 1, 3, and 10 μ s.

gap. Each of the voltage sources generates a Gaussian pulse specified by the following expression:

$$V(t) = 1000 \exp \left[-\left(\frac{\beta}{\tau_0}\right)^2 (t - \tau_0)^2 \right]$$
 [V] (1)

where β was set to 2.5 and three different values of τ_0 were used. The corresponding half-peak width (HPW) can be found as

$$HPW = \frac{2 \tau_0 \sqrt{\ln 2}}{\beta} \quad [s]$$
 (2)

When $\beta=2.5$ and $\tau_0=1.5$, 4.5 or 15 μ s, HPWs are 1, 3, or 10 μ s, respectively. Fig. 2 shows waveforms of the voltage generated by each of the voltage sources for those three values of HPW. This type of excitation is also known as delta-gap electric-field excitation (e.g., Balanis [18]). Note that the delta-gap electric-field excitation generates electric field across the gap regardless of the current flowing there; that is, in effect, it acts as a voltage source with zero internal impedance.

We additionally performed simulations for the same cylinder, but excited by a current source (azimuthal magnetic field at $r=100.5\,\mathrm{m}$). The results were essentially the same.

We computed current waveforms, as well as longitudinal, E_z , and radial, E_T , electric field waveforms, at distances of 100, 300, and 500 m from the source. The corresponding magnetic fields and Poynting vectors were also computed. Some current waveforms at z=100 m exhibit an appreciable opposite polarity overshoot, which we attribute to the proximity to the source region, where stronger scattering is expected [1]. Current HPW at z=100 m is similar to that of the excitation voltage waveform. Current risetimes at z=100 m are similar to those expected for CIDs [14].

III. ANALYSIS AND RESULTS

Fig. 3(a), (b), (c), and (d) shows, on a 5- μ s time scale, FDTD-computed waveforms of current carried by the cylinder at z=100, 300, and 500 m from the source for voltage pulse HPW = 1 μ s and $\sigma=\infty, 10^{-3}$ S/m, 10^{-4} S/m, and 10^{-5} S/m, respectively. Fig. 4 is the same as Fig. 3, but for HPW = 3 μ s and shown on a 10- μ s time scale. Fig. 5 is the same as Fig. 3, but for HPW = 10 μ s and shown on a 50- μ s time scale. Note that the vertical scales of Figs. 3(d), 4(d), and 5(d) for $\sigma=$

10

10

10

10

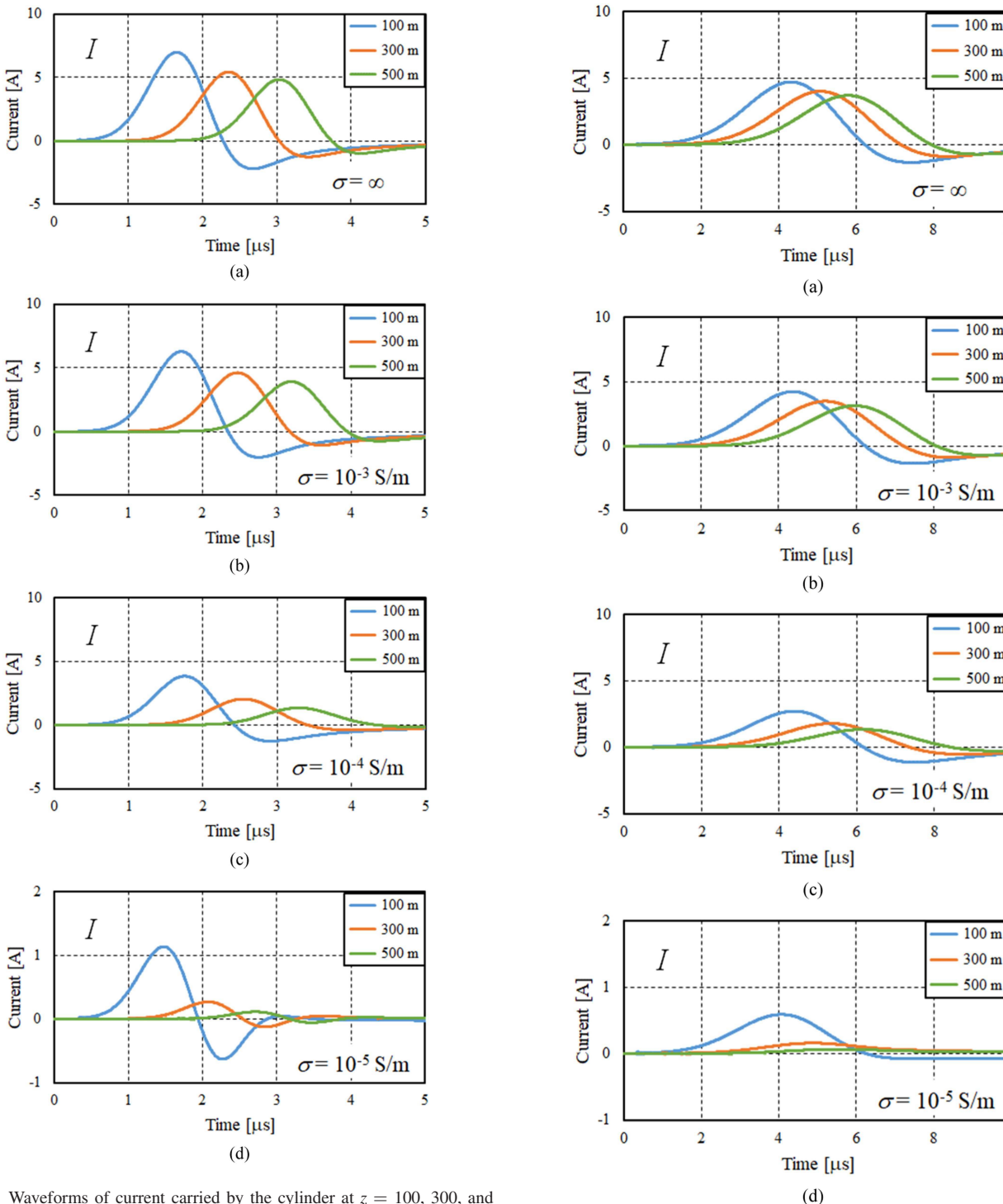


Fig. 3. Waveforms of current carried by the cylinder at z=100, 300, and 500 m from the source for (a) $\sigma=\infty$, (b) $\sigma=10^{-3}$ S/m, (c) $\sigma=10^{-4}$ S/m, and (d) $\sigma=10^{-5}$ S/m, shown on a 5- μ s time scale. Voltage HPW = 1 μ s. Note that the vertical scale in (d) is different from that in (a), (b), and (c).

Fig. 4. Same as Fig. 3, but for voltage HPW = 3 μs and shown on a 10- μs time scale.

 10^{-5} S/m are different from those of the other three panels. Currents were computed from azimuthal magnetic fields as $I=2~\pi~r~H_{\varphi}$ for r=100.5 m. Note that the current computed in this manner can include both conduction and displacement components. For each of the four values of σ , a traveling current wave is detectable in Figs. 3, 4, and 5. Further, the current wave attenuates as it moves along the cylinder away from the source,

even when $\sigma=\infty$. As shown in [1], this attenuation is caused by the opposite-polarity current induced by the longitudinal electric field. When HPW = 10 μ s and $\sigma=\infty$ or 10^{-3} S/m [see Fig. 5(a) and (b)], current waves reflected from the ends of the cylinder, each terminated in a perfectly conducting plane, are seen around 35 μ s (about 20 μ s after the arrival of the incident current wave). Note that reflected current waves can freely

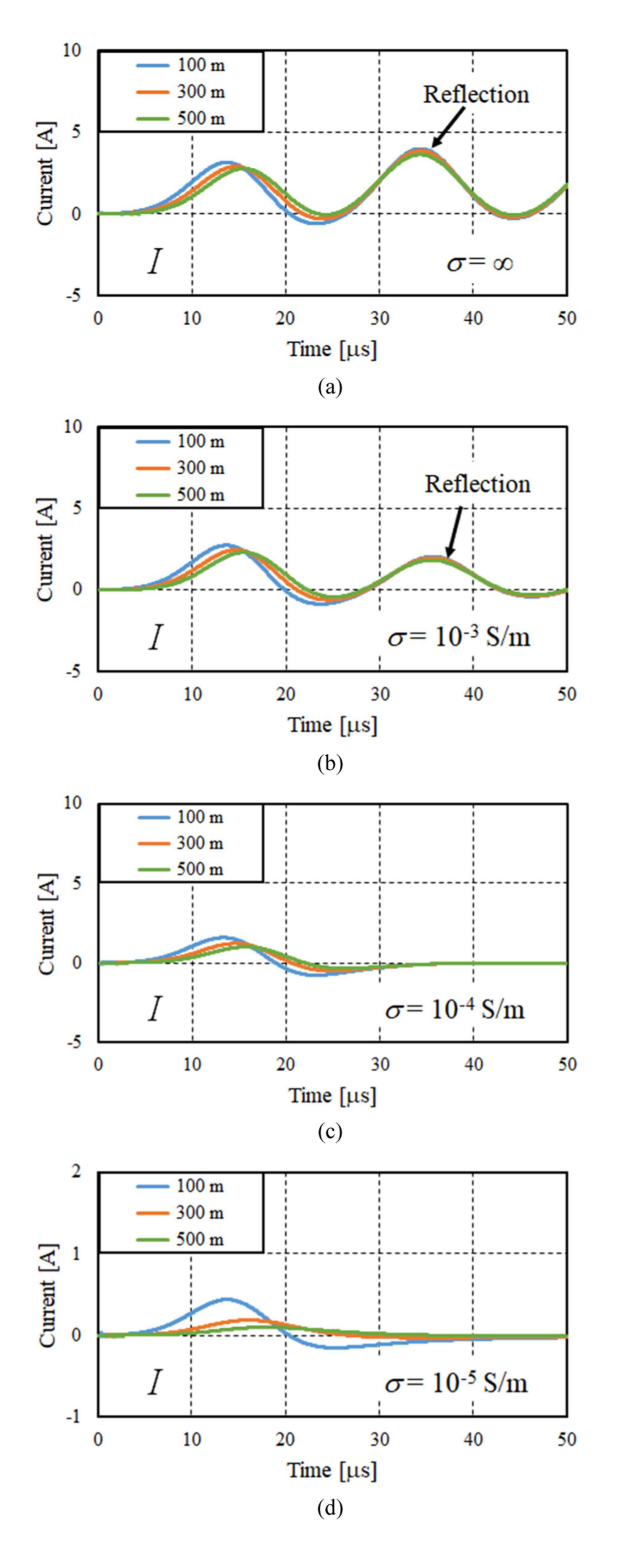


Fig. 5. Same as Fig. 3, but for voltage HPW = 10μ s and shown on a $50-\mu$ s time scale. Reflections from the 6-km long cylinder ends are seen in (a) and (b).

traverse the 1-m delta-gap source, which acts as an ideal voltage source.

We estimated the characteristic frequency for each of the three excitation voltage pulses, simply defined here as $f_c=1/(4RT)$, where RT is the voltage pulse risetime. For the cylinder with $\sigma=10^{-3}$ S/m, $\sigma>>2\pi f_c\varepsilon_0$ (= 2.2×10^{-6} to 2.1×10^{-5}) for all the

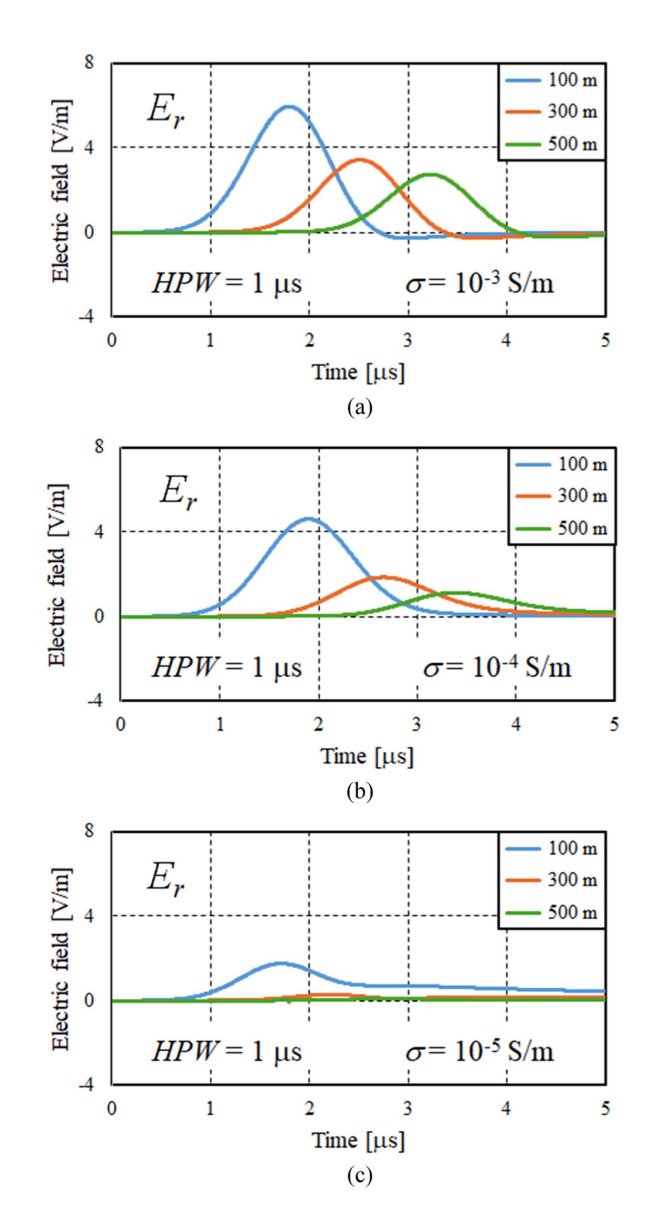


Fig. 6. Waveforms of radial (normal) electric field E_{τ} on the cylinder surface at $z=100,\,300,\,$ and 500 m from the source for (a) $\sigma=10^{-3}$ S/m, (b) $\sigma=10^{-4}$ S/m, and (c) $\sigma=10^{-5}$ S/m, respectively. Voltage HPW = 1 μ s.

three characteristic frequencies ranging from 40 to 370 kHz, and hence such a cylinder can be viewed as a good conductor. For the cylinder with $\sigma=10^{-4}$ S/m, σ is by a factor of about 5 to 50 higher than $2\pi f_c \varepsilon_0$ for 40 to 370 kHz, respectively, so that it can be reasonably viewed as a fairly good conductor. The cylinder with $\sigma=10^{-5}$ S/m is not a good conductor for any characteristic frequency. However, as seen in Figs. 3(d), 4(d), and 5(d), that cylinder is still capable of supporting the propagation of current waves, although with strong attenuation.

Fig. 6(a), (b), and (c) shows FDTD-computed waveforms of radial (normal) electric field E_r on the cylinder surface at z=100, 300, and 500 m from the source for HPW = 1 μ s and $\sigma=10^{-3}$, 10^{-4} , and 10^{-5} S/m, respectively. Although the waveforms of E_r for $\sigma=\infty$ are not shown here, they are similar to those for $\sigma=10^{-3}$ S/m. The peak of E_r decreases with decreasing σ .

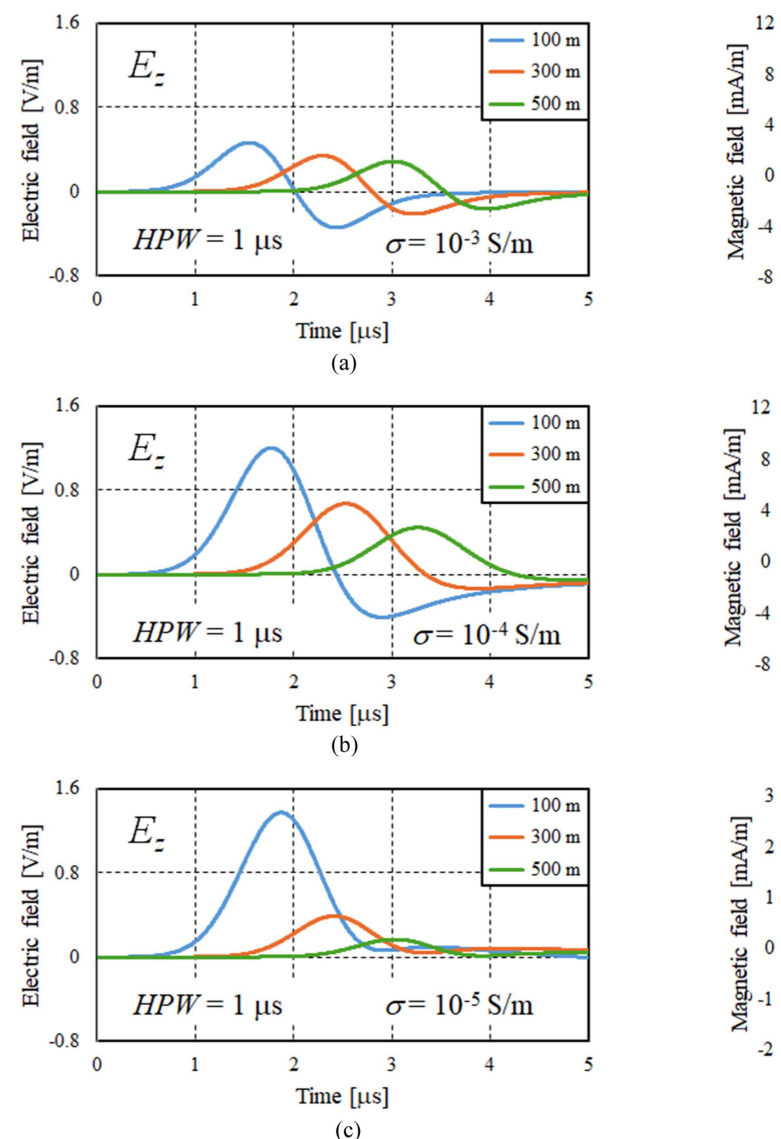


Fig. 7. Same as Fig. 6, but for the longitudinal (tangential) electric field E_z on the cylinder surface. Voltage HPW = 1 μ s.

Fig. 7(a), (b), and (c) shows FDTD-computed waveforms of longitudinal (tangential) electric field E_z on the cylinder surface at z=100, 300, and 500 m from the source for HPW = 1 μ s and $\sigma=10^{-3}$, 10^{-4} , and 10^{-5} S/m, respectively. Note that $E_z=0$ for $\sigma=\infty$. As expected, the peak of E_z increases with decreasing σ . It follows from comparison of E_r shown in Fig. 6 and E_z shown in Fig. 7 that E_r is a factor of 10 to 55 higher than E_z for $\sigma=10^{-3}$ S/m. The ratio E_r/E_z ranges from 3 to 10 for $\sigma=10^{-4}$ S/m and from 0.6 to 3 for $\sigma=10^{-5}$ S/m. Note that the ratio E_r/E_z decreases with increasing the distance from the excitation point and with decreasing the voltage-pulse HPW, so that the lower-bound values above correspond to larger distances and smaller HPWs.

Fig. 8(a), (b), and (c) shows FDTD-computed waveforms of azimuthal magnetic field H_{φ} on the cylinder surface at z=100, 300, and 500 m from the source for HPW = 1 μ s and $\sigma=10^{-3}$,

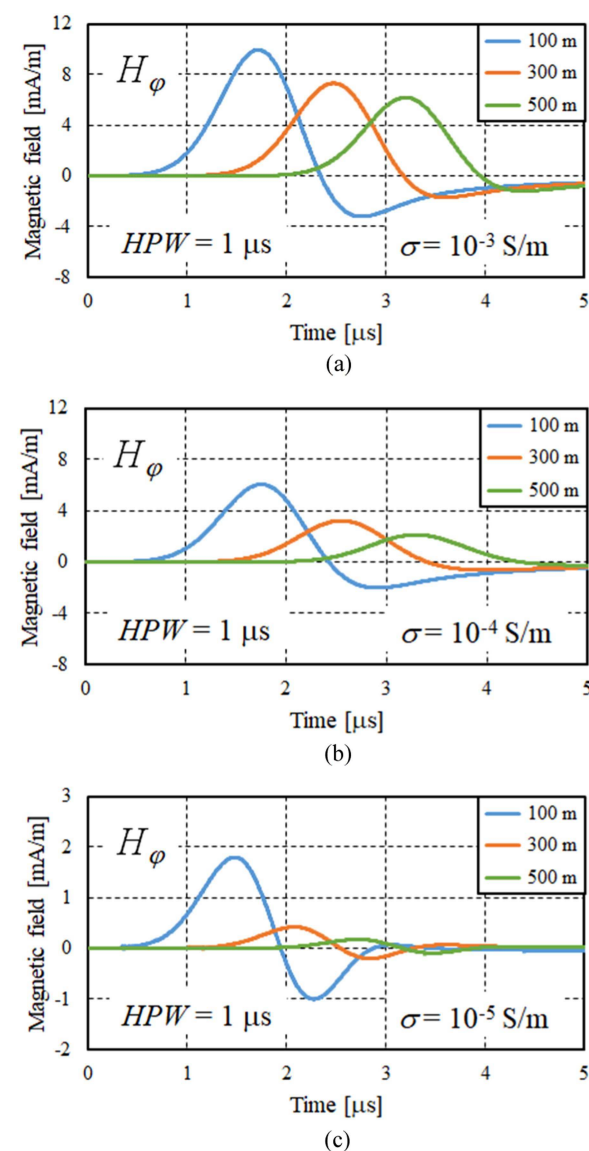


Fig. 8. Waveforms of azimuthal magnetic field H_{φ} on the cylinder surface at 100, 300, and 500 m from the source for (a) $\sigma=10^{-3}$ S/m, (b) $\sigma=10^{-4}$ S/m, and (c) $\sigma=10^{-5}$ S/m. Voltage HPW = 1 μ s. The shapes of the H_{φ} waveforms are the same as those of the corresponding current waveforms in Fig. 3(b), (c), and (d). Note that the vertical scale in (c) is different from that in (a) and (b).

 10^{-4} , and 10^{-5} S/m, respectively. The waveforms of H_{φ} for $\sigma = \infty$, not shown here, are similar to those for $\sigma = 10^{-3}$ S/m.

Fig. 9(a), (b), and (c) shows waveforms of longitudinal Poynting vector $P_z = E_r \times H_\varphi$ on the cylinder surface at z = 100, 300, and 500 m from the source for $\sigma = 10^{-3}$, 10^{-4} , and 10^{-5} S/m, respectively. The waveforms of P_z for $\sigma = \infty$, not shown here, are similar to those for $\sigma = 10^{-3}$ S/m. It follows from Fig. 9 that P_z (power flow density along the cylinder) decreases with decreasing σ . Fig. 10(a), (b), and (c) shows waveforms of radial (normal) component of Poynting vector $P_r = E_z \times H_\varphi$ on the cylinder surface at z = 100, 300, and 500 m from the source for $\sigma = 10^{-3}$, 10^{-4} , and 10^{-5} S/m, respectively. It follows from Fig. 10 that P_r increases with decreasing σ . The ratio P_z/P_r

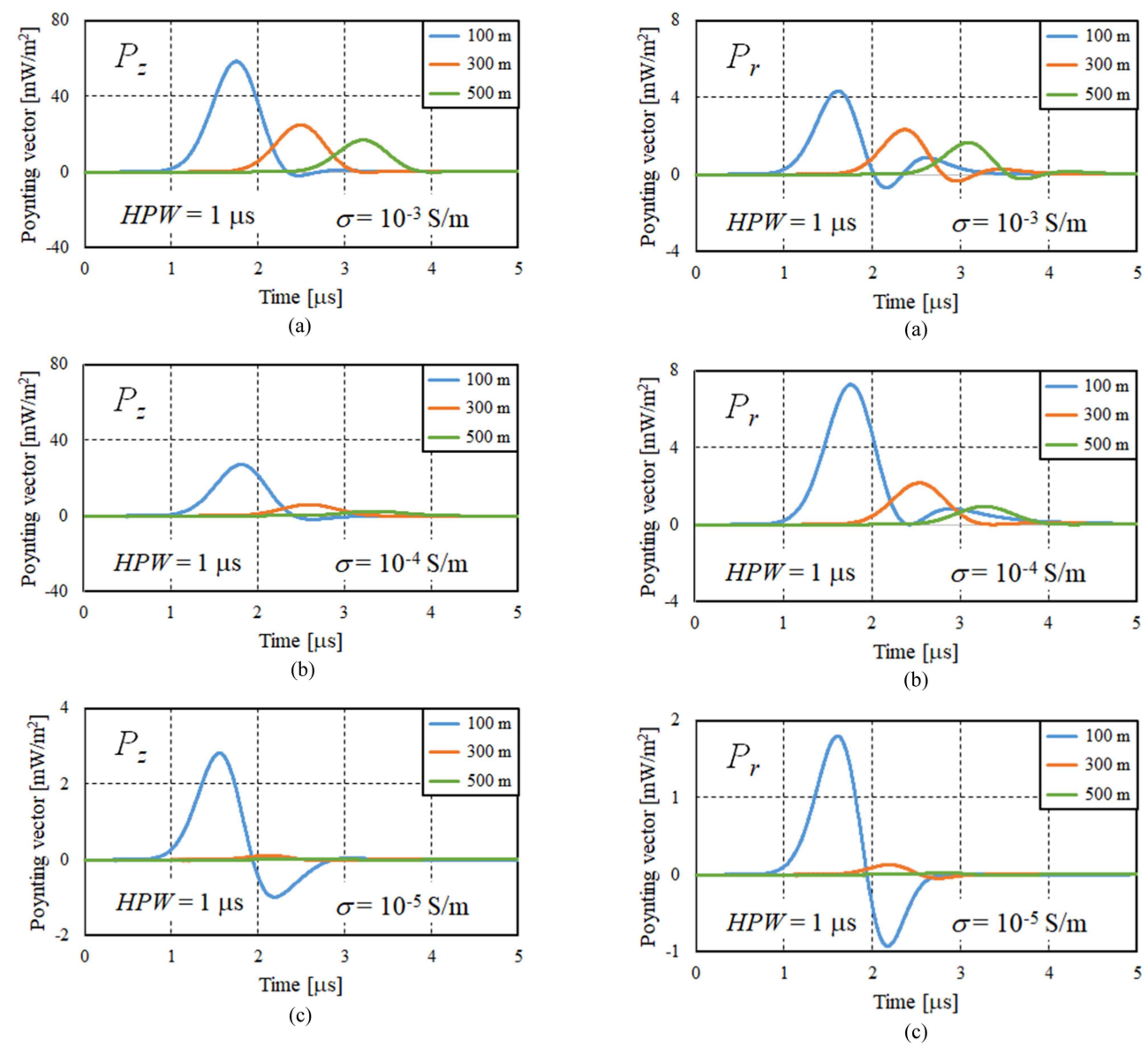


Fig. 9. Waveforms of longitudinal (along the cylinder) component of Poynting vector $P_z = E_T \times H_\varphi$ on the cylinder surface at z=100,300, and 500 m from the source for HPW = 1 μ s and (a) $\sigma=10^{-3}$ S/m, (b) $\sigma=10^{-4}$ S/m, and (c) $\sigma=10^{-5}$ S/m. Note that the vertical scale in (c) is different from that in (a) and (b).

Fig. 10. Same as Fig. 9, but for the radial (normal to the cylindrical surface) component of Poynting vector $P_r = E_z \times H_{\varphi}$. Note that for $\sigma = \infty$, $P_r = 0$. Note that the vertical scale in (c) is different from that in (a) and (b).

ranges from 10 to 54 for $\sigma = 10^{-3}$ S/m, from 3 to 10 for $\sigma = 10^{-4}$ S/m, and from 0.7 to 2.7 for 10^{-5} S/m. For each range, the larger value corresponds to 100 m.

IV. DISCUSSION

Table I gives current wave propagation speeds, v, evaluated from the peak-to-peak time intervals corresponding to propagation from z=100 m to z=300 m and from z=300 m to z=500 m for different values of σ and voltage pulse HPW. It follows from Table I that v is between 140 and 290 m/ μ s (0.47c and 0.97c) for $\sigma \geq 10^{-4}$ S/m and that it decreases with decreasing σ and with increasing HPW. Note that, because of the scattering effect [1], even for $\sigma = \infty$ the propagation speed is lower than the speed of light. For $\sigma = 10^{-5}$ S/m and voltage-pulse

HPW = 1 μ s, v slightly exceeds c, which is probably due to uncertainties in identifying the peaks of attenuated current waveforms at z = 300 and 500 m.

Fig. 11(a), (b), and (c) shows peaks of current wave at z=300 and 500 m in percent of that at z=100 m, for $\sigma=\infty$, 10^{-3} S/m, 10^{-4} S/m, and 10^{-5} S/m and for three different voltage-pulse HPWs: 1, 3, and 10 μ s, respectively. It follows from Fig. 11 that the current peak decreases with distance, and the decrease is more significant for smaller voltage-pulse HPW (higher characteristic frequency f_c). The attenuation rates for $\sigma=\infty$ and $\sigma=10^{-3}$ S/m are very similar. Stronger attenuation for $\sigma=10^{-4}$ and 10^{-5} S/m is due, at least in part, to ohmic losses (R=0.32 Ω /m and 3.2 Ω /m, respectively). For HPW = 10 μ s ($f_c=40$ kHz), the reduction of peak current after its traveling over 400 m (from 100 to 500 m) is about 10%

TABLE I CURRENT WAVE PROPAGATION SPEEDS, v, EVALUATED FROM THE PEAK-TO-PEAK TIME INTERVALS CORRESPONDING TO PROPAGATION FROM z=100 to 300 m and From z=300 to 500 m for Different Values of σ and Voltage Pulse HPW

σ, S/m	z = 100 to 300 m			z = 300 to 500 m		
	Voltage pulse HPW			Voltage pulse HPW		
	1 μs	3 μs	10 μs	1 μs	3 μs	10 μs
	290	260	210	290	280	250
10^{-3}	270	240	200	280	260	230
10^{-4}	250	210	140	270	240	180
10-5	~300	250	90	~300	300	110

for $\sigma = \infty$, about 20% for $\sigma = 10^{-3}$ S/m, about 40% for $\sigma = 10^{-4}$ S/m, and about 80% for $\sigma = 10^{-5}$ S/m. In the "worst" case, $\sigma = 10^{-5}$ S/m and HPW = 1 μ s ($f_c = 370$ kHz), the current peak is about 20% at 300 m and about 10% at 500 m of its value at 100 m. For an isolated cylinder section, whose length is equal to 400 m (a rather typical value for CIDs), the computed non-zero current at its far end means that the current wave would necessarily be reflected with the opposite sign (as from an open circuit). For a 200-m long section, the current reflection would be stronger [compare current magnitudes at 500 m and 300 m in Fig. 11(a), (b), and (c)].

If we assume that the current decay with distance is exponential, then the attenuation distances, over which the amplitude decreases to 1/e (about 37%) of its original value, for $\sigma=10^{-5}$ S/m will be roughly 120, 170, and 220 m for HPW = 1, 3, and 10 μs , respectively. For comparison, Li et al. [10], who modeled two CIDs reported by Rison et al. [9], inferred the attenuation distances of 375 and 379 m, corresponding to CID lengths of 720 and 412 m, respectively.

Since the model employed in this article is linear, the results can be scaled up to higher currents. For example, an increase of the excitation voltage peak from 1 kV to 1 MV would lead to an increase of current peak at z=100 m from 3.8 A to 3.8 kA for HPW = 1 μ s and $\sigma=10^{-4}$ S/m. In the case of current-source excitation, scaling up in terms of current can be done directly.

We now briefly discuss our assumption that the conductivity of CIDs (essentially cold streamer formations) is of the order of 10^{-5} S/m. This assumption is based on the following three works in which conductivity of different streamer formations in lightning and long sparks was estimated. Maslowski and Rakov [11], using measured radial electric field in the immediate vicinity of the lightning channel and measured channel base current, along with three TL-type models specifying different current decay with height, estimated the corona sheath conductivity to be of the order of 10^{-6} – 10^{-5} S/m. The corona sheath surrounding the narrow hot channel core is formed via streamer discharges during the leader stage and it is subsequently neutralized via the so-called reverse corona during the return-stroke stage. The bulk of the corona sheath, whose radial dimension is of the order of meters or more, is composed of essentially cold streamers. Rakov and Tran [12] estimated conductivity of a common streamer zone for one rocket-and-wire triggered lightning discharge. They used the dimensions of the common streamer zone, roughly estimated from the high-speed video record (cross-sectional area $A = 20 \text{ m}^2$), the corresponding

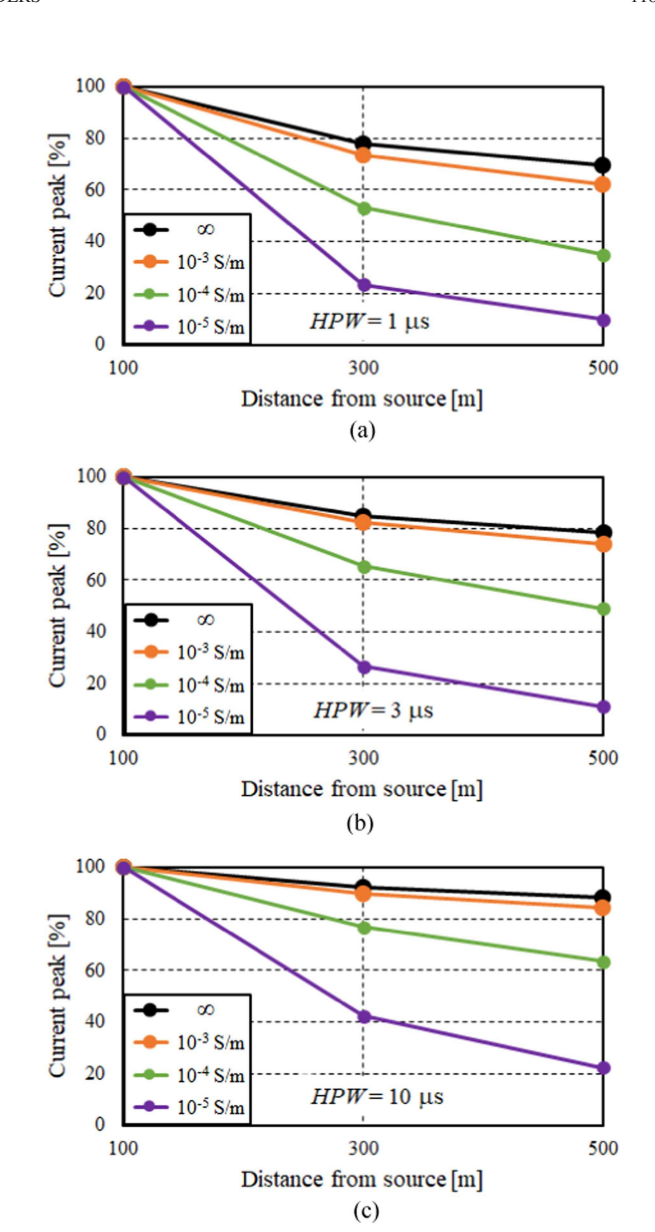


Fig. 11. Peaks of current wave at z=300 and 500 m in percent of that at z=100 m, for $\sigma=\infty$, 10^{-3} , 10^{-4} , and 10^{-5} S/m and for three different voltage-pulse HPWs: (a) 1 μ s, (b) 3 μ s, and (c) 10 μ s. Note that the total propagation distance here is 400 m.

measured current I=600 A, and the expected longitudinal electric field E=1.0 MV/m in common streamer zone [3], with the resultant conductivity value being 3×10^{-5} S/m. Bogatov et al. [13], who studied the streamer zone of positive leaders in a 5.5-m long rod-plane gap, reported conductivity on the axis of streamer zone during the initial stage of the breakthrough phase to be about 2×10^{-5} S/m. They arrived at that value using the streamer density estimated from optical records, measured discharge current, and typical electric field in positive streamer zone (0.5 MV/m). They also found that conductivity during the breakthrough phase tended to increase with time, but remained of the order of 10^{-5} S/m. It is remarkable how the above studies of different streamer formations yielded similar values of conductivity, of the order of 10^{-5} S/m. Since CIDs are presently thought to be essentially cold streamer formations [9], we find it

reasonable to extrapolate this latter conductivity value to CIDs. We are not aware of any other estimates of conductivity for streamer formations.

V. SUMMARY

Using the FDTD method for solving Maxwell's equations, we have studied wave guiding properties of a large cylinder, which has a radius of 100 m, $\varepsilon = \varepsilon_0$, and $\mu = \mu_0$, for four values of conductivity, $\sigma = \infty$, 10^{-3} S/m, 10^{-4} S/m, and 10^{-5} S/m. The conductivity value of the order of 10^{-5} S/m is expected for various essentially cold streamer formations [11], [12], [13], including CIDs, with the other three values being considered just for comparison. The cylinder was excited by a Gaussian voltage pulse whose HPW was 1, 3, or $10~\mu s$ (excitation by a current pulse yielded essentially the same results). The characteristic frequencies of excitation pulse ranged from 40 to 370 kHz. Currents, electric and magnetic fields, and Poynting vectors were computed at 100, 300, and 500 m from the source. Our findings can be summarized as follows.

- In all considered cases, the cylinder was capable of guiding current waves, with the propagation speed being of the order of 10⁸ m/s.
- 2) The wave guiding properties of the cylinder with $\sigma = 10^{-3}$ S/m were very similar to those of perfectly conducting cylinder.
- 3) The radial electric field E_{τ} on the cylinder surface was a factor of 10 to 55 higher than the longitudinal electric field E_z for $\sigma=10^{-3}$ S/m, a factor of 3 to 10 higher for $\sigma=10^{-4}$ S/m, and ranged from 0.6 to 3 for $\sigma=10^{-5}$ S/m (smaller values correspond to larger distances from the excitation point and smaller voltage-pulse HPWs).
- 4) The ratio of the longitudinal Poynting vector P_z on the cylinder surface to the radial Poynting vector P_r is almost the same as the corresponding ratio E_τ/E_z , since $P_z=E_r\times H_\varphi$ and $P_r=E_z\times H_\varphi$.
- 5) After propagation over 400 m, the current peak was about 70% to 90% of its original value for $\sigma = \infty$, about 60% to 80% for $\sigma = 10^{-3}$ S/m, about 40% to 60% for $\sigma = 10^{-4}$ S/m, and about 10% to 20% for $\sigma = 10^{-5}$ S/m.
- 6) The current attenuation distances, over which the amplitude decreases to 1/e (about 37%) of its original value, for $\sigma = 10^{-5}$ S/m were roughly 120, 170, and 220 m for HPW = 1, 3, and 10 μ s, respectively.

Our results, based on a full-wave solution of Maxwell's equations, suggest that CIDs that are essentially cold streamer formations, whose conductivity is expected to be about 10^{-5} S/m and whose lengths are usually a few hundreds of meters, may involve traveling wave phenomena, such as reflections.

REFERENCES

- [1] Y. Baba and V. A. Rakov, "On the mechanism of attenuation of current waves propagating along a vertical perfectly conducting wire above ground: Application to lightning," *IEEE Trans. Electromagn. Compat.*, vol. 47, no. 3, pp. 521–532, Aug. 2005.
- [2] M. A. Uman and D. K. McLain, "Magnetic field of lightning return stroke," J. Geophys. Res., vol. 74, no. 28, pp. 6899–6910, Dec. 1969.
- [3] B. N. Gorin, "Mathematical modeling of lightning return stroke (in Russian)," *Elektrichestvo*, no. 4, pp. 10–16, 1985.

- [4] V. A. Rakov and M. A. Uman, "Lightning: Physics and Effects," Cambridge, U.K.: Cambridge Univ. Press, 2003, Art. no. 687.
- [5] A. Nag and V. A. Rakov, "Compact intracloud lightning discharges: 1. Mechanism of electromagnetic radiation and modeling," *J. Geophys. Res.*, vol. 115, no. D20102, 2010, Art. no. 20.
- [6] A. De Conti, F. H. Silveira, S. Visacro, and T. C. M. Cardoso, "A review of return-stroke models based on transmission line theory," *J. Atmos. Sol.-Terr. Phys.*, vol. 136, no. Part A, pp. 52–60, Dec. 2015.
- [7] M. D. Tran and V. A. Rakov, "An advanced model of lightning M-component," J. Geophys. Res., Atmos., vol. 124, no. 4, pp. 2296–2317, Feb. 2019.
- [8] V. A. Rakov, "Some inferences on the propagation mechanisms of dart leaders and return strokes," *J. Geophys. Res.*, vol. 103, no. D2, pp. 1879–1887, 1998.
- [9] W. Rison et al., "Observations of narrow bipolar events reveal how lightning is initiated in thunderstorms," *Nature Commun.*, vol. 7, 2016, Art. no. 10721.
- [10] D. Li et al., "Secondary fast breakdown in narrow bipolar events," *Geophys. Res. Lett.*, vol. 49, no. 7, Apr. 2022, Art. no. e2021GL097452.
- [11] G. Maslowski and V. A. Rakov, "A study of the lightning channel corona sheath," J. Geophys. Res., vol. 111, no. D14110, p. 16, Jul. 2006.
- [12] V. A. Rakov and M. D. Tran, "The breakthrough phase of lightning attachment process: From collision of opposite-polarity streamers to hot-channel connection," *Electric Power Syst. Res.*, vol. 173, pp. 122–134, Aug. 2019.
- [13] N. A. Bogatov et al., "Experimental investigation of the streamer zone of long-spark positive leader using high-speed photography and microwave probing," *J. Geophys. Res.*, Atmos., vol. 125, no. 11, Jun. 2020, Art. no. e2019JD031826.
- [14] A. Nag and V. A. Rakov, "Compact intracloud lightning discharges: 2. Estimation of electrical parameters," *J. Geophys. Res.*, vol. 115, no. D20103, p. 15, Oct. 2010.
- [15] K. S. Yee, "Numerical solution of initial boundary value problems involving Maxwell's equations in isotropic media," *IEEE Trans. Antennas Propag.*, vol. 14, no. 3, pp. 302–307, 1996.
- [16] V. A. Rakov et al., "New insights into the lightning discharge processes," Plasma Sources Sci. Technol., vol. 31, no. 10, 2022, Art. no. 104005.
- [17] Z. P. Liao, H. L. Wong, B. P. Yang, and Y. F. Yuan, "A transmission boundary for transient wave analysis," *Sci. China, Ser. A*, vol. A27, no. 10, pp. 1063–1076, 1984.
- [18] C. A. Balanis, Antenna Theory: Analysis and Design, 2nd ed. Hoboken, NJ, USA: Wiley, 1997.



Shota Ueda received the B.Sc. degree in electrical engineering from Doshisha University, Kyoto, Japan, in 2024.

His research interest includes Computational Electromagnetics.



Masahiro Hasegawa received the B.Sc. degree in electrical engineering from Doshisha University, Kyoto, Japan, in 2022.

His research interest includes Computational Electromagnetics.



Yoshihiro Baba (Fellow, IEEE) received the B.Sc., M.Sc., and Ph.D. degrees in electrical engineering from the University of Tokyo, Tokyo, Japan, in 1994, 1996 and 1999, respectively.

Since 2012, he has been a Professor with Doshisha University, Kyoto, Japan. From 2022 to 2024, he was the Dean of the Institute of Advanced Research and Education, Doshisha University. Since 2024, he has been the Director of the Center for Learning Support and Faculty Development, Doshisha University. From 2003 to 2004, he was a Visiting Scholar with the

University of Florida. He is the author or coauthor of four books, seven book chapters, and more than 130 papers published in reviewed international journals.

Dr. Baba was the receipient of the Technical Achievement Award from the IEEE EMC Society in 2014. He was an Editor for IEEE TRANSACTION POWER DELIVERY from 2009 to 2018, and an Associate Editor for *Electrical Engineering* (Springer Journal) from 2019 to 2022. He has been an Associate Editor for IEEE TRANSACTIONS ON ELECTROMAGNETIC COMPATIBILITY since 2022. He is a Fellow of the Institution of Engineering and Technology and of the Institute of Electrical Engineers of Japan.



Vladimir A. Rakov (Fellow, IEEE) received the M.S. and Ph.D. degrees in electrical engineering from the Tomsk Polytechnical University (Tomsk Polytechnic), Tomsk, Russia, in 1977 and 1983, respectively.

From 1977 to 1979, he was an Assistant Professor of electrical engineering with Tomsk Polytechnic. In 1978, he joined with the High Voltage Research Institute (a division of Tomsk Polytechnic), where from 1984 to 1994, he was the Director of the Lightning Research Laboratory. He is currently a Distinguished Professor with the Department of Electrical and Com-

puter Engineering, University of Florida, Gainesville, FL, USA, and the Director of the International Center for Lightning Research and Testing. He is the author or coauthor of five books, and more than 900 other publications on various aspects of lightning, with over 360 papers being published in reviewed journals.

Dr. Rakov is a Fellow of four major professional societies, IEEE, the American Geophysical Union, the American Meteorological Society, and the Institution of Engineering and Technology.